RESEARCH ARTICLE

Atmospheric mercury in the Latrobe Valley, Australia: Case study June 2013

Robyn Schofield[1,2,*], Steven Utembe[1,3], Caitlin Gionfriddo[1,4], Michael Tate[5], David Krabbenhoft[5], Samuel Adeloju[6,7], Melita Keywood[8,9], Roger Dargaville[1,10], and Mike Sandiford[1]

Gaseous elemental mercury observations were conducted at Churchill, Victoria, in Australia from April to July, 2013, using a Tekran 2537 analyzer. A strong diurnal variation with daytime average values of 1.2–1.3 ng m^{-3} and nighttime average values of 1.6–1.8 ng m^{-3} was observed. These values are significantly higher than the Southern Hemisphere average of 0.85–1.05 ng m^{-3}. Churchill is in the Latrobe Valley, approximately 150 km East of Melbourne, where approximately 80% of Victoria's electricity is generated from low-rank brown coal from four major power stations: Loy Yang A, Loy Yang B, Hazelwood, and Yallourn. These aging generators do not have any sulfur, nitrogen oxide, or mercury air pollution controls. Mercury emitted in the 2015–2016 year in the Latrobe Valley is estimated to have had an externalized health cost of $AUD88 million. Air pollution mercury simulations were conducted using the Weather Research and Forecast model with Chemistry at 3 × 3 km resolution. Electrical power generation emissions were added using mercury emissions created from the National Energy Market's 5-min energy distribution data. The strong diurnal cycle in the observed mercury was well simulated ($R^2 = .49$ and P value $= 0.00$) when soil mercury emissions arising from several years of wet and dry deposition in a radius around the power generators was included in the model, as has been observed around aging lignite coal power generators elsewhere. These results indicate that long-term air and soil sampling in power generation regions, even after the closure of coal fired power stations, will have important implications to understanding the airborne mercury emissions sources.

Keywords: Gaseous elemental mercury, Air mercury, Coal power generation, Soil

1. Introduction

Australia is one of the original 128 signatories to the UNEP Minamata convention on mercury signed on January 13, 2013. Minamata is a city in Japan infamous for its devastating mercury poisoning of its inhabitants, and the convention is designed to protect human health and the environment from the adverse effects of mercury (http://mercuryconvention.org/). As of November 17, 2020, 125 countries have ratified the Minamata treaty, which came into force on August 16, 2017. Australia is among the remaining 34 original signatories yet to ratify the convention. The control of the anthropogenic releases of mercury throughout its life cycle is a key component of the obligations under the convention.

Mercury readily vaporizes and in its elemental form undergoes global transport residing in the atmosphere for up to 1 year (Selin et al., 2007). Human activities have increased the atmospheric concentration of mercury by 5.5–7.6 times the natural baseline, and the deposition enhancement ranges between 3 and 5-fold (Biester et al., 2007; Amos et al., 2013; Outridge et al., 2018, and references therein). Australian mercury emissions from natural and human activities of both diffuse and stationary nature are provided in **Figure 1** for 2015/2016 from

[1] School of Earth Sciences, University of Melbourne, Melbourne, Victoria, Australia

[2] ARC Centre of Excellence for Climate Extremes, University of Melbourne, Melbourne, Victoria, Australia

[3] Environmental Protection Agency, Macleod, Victoria, Australia

[4] Biosciences Division, Oak Ridge National Laboratory, Oak Ridge, TN, USA

[5] Wisconsin Water Science Center, US Geological Survey, Middleton, WI, USA

[6] School of Chemistry, Monash University, Melbourne, Victoria, Australia

[7] Charles Sturt University, Albury, New South Wales, Australia

[8] Federation University, Churchill, Victoria, Australia

[9] CSIRO Oceans and Atmosphere Business Unit, Aspendale, Victoria, Australia

[10] Department of Civil Engineering, Monash University, Melbourne, Victoria, Australia

* Corresponding author:
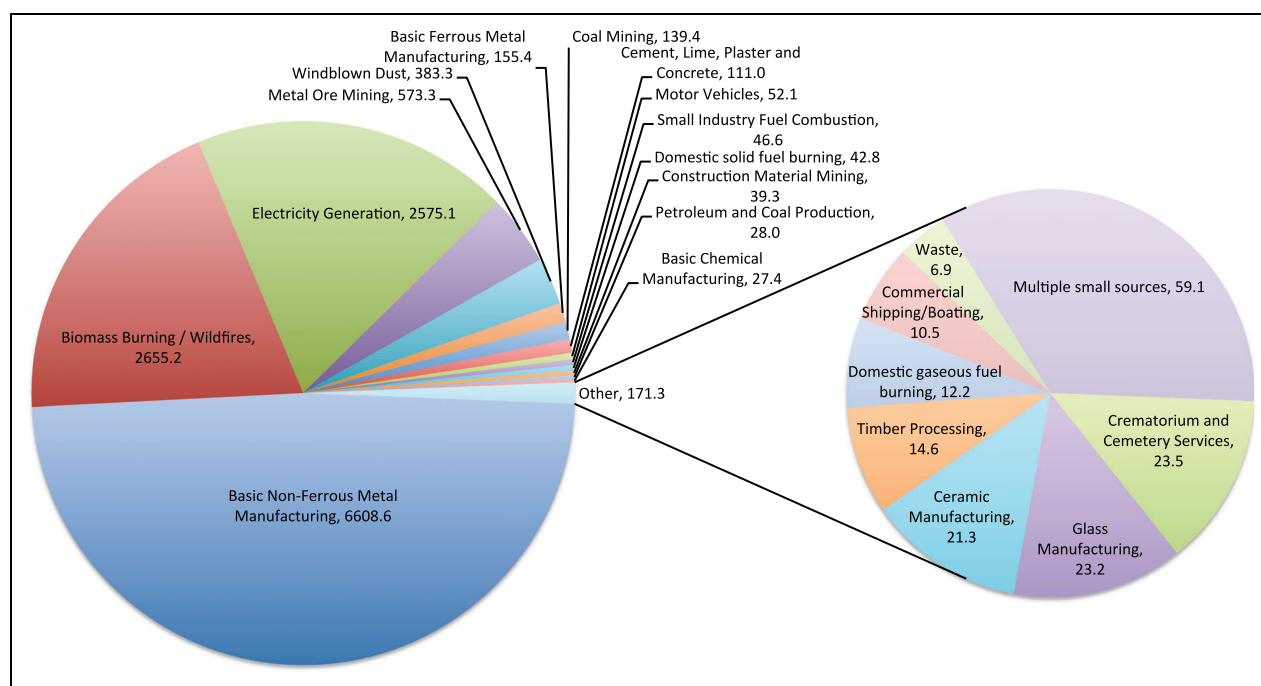Email: robyn.schofield@unimelb.edu.au

Figure 1. Australian National Pollution Inventory data for atmospheric gaseous mercury emissions (kg) for the financial year of 2015–2016. The mercury emissions from the paved/unpaved road source were not included because the brief suspension in the air of particulate mercury within road dust and subsequent resettling is not a source of gaseous mercury to the atmosphere. DOI: https://doi.org/10.1525/elementa.2021.00072.f1

the National Pollution Inventory (NPI; www.npi.gov.au). Note that the large paved/unpaved road emissions (almost 9 tonnes of mercury) represents mercury in road dust which, while briefly suspended with road use, resettles again quickly within minutes, so it does not make a significant contribution to atmospheric mercury concentrations; therefore, it is not included in the budget shown in **Figure 1**.

The need for intensive monitoring campaigns focused on atmospheric mercury and its oxidants is widely recognized (Dommergue et al., 2010). In Australia, and the Southern Hemisphere generally, there has in recent years been increased efforts to conduct atmospheric mercury measurements (Nelson, 2007; Nelson et al., 2011; Slemr et al., 2015; Sprovieri et al., 2016; Howard et al., 2017; Martin et al., 2017; Howard and Edwards, 2018; Howard et al., 2019; Bieser et al., 2020; Slemr et al., 2020). Tropical measurements made in Northern Australia near Darwin from 2014 to 2016 displayed higher average gaseous elemental mercury (GEM) in the late dry season (August to late November) of 0.99 ng m^{-3} (mean over 2014 and 2015) consistent with enhanced emissions from biomass burning in the late dry season (Howard et al., 2017). Decreasing GEM values are seen with the wet season progression with mean values in March of 0.76 and 0.88 ng m^{-3} for 2014 and 2015, respectively (Howard et al., 2017). In contrast, at the Southern mid-latitude site Cape Point, South Africa (background) GEM measurements ranged from 0.913 to 1.108 ng m^{-3} (2007–2014), which were able to be described by a simple empirical formula dependent on the annual rainfall rate (RR) GEM = 0.0002 × RR + 0.978 (Brunke et al., 2016). Early data (2011–2013) from the long-term measurements of GEM at Cape Grim in NW Tasmania were reported in

Slemr et al. (2015), foundannual average GEM concentrations ranged from 0.85 to 0.96 ng m^{-3}.

Here, we describe the first measurements of GEM for the Latrobe Valley in the state of Victoria, in South-Eastern Australia. The Latrobe Valley supplies 80% of Victoria's electricity from brown coal combustion. Although Australian coal is considered to have low mercury content, the mercury emissions provided in the NPI, and the poor energy efficiency of brown coal, requiring more coal to be burnt per kWh produced, means the Latrobe Valley produces significant mercury emissions (**Table 1**). Further, the absence of co-beneficial removal of mercury in Australia through air pollution control of sulfur dioxide or oxides of nitrogen, that is, sulfur scrubbers and so on (Pacyna et al., 2010), as is standard practice elsewhere (i.e., Europe, United States, and China), means that most of the mercury in the coal used in the Australian electricity production is released to the atmosphere. **Table 1** shows that these aging coal power stations represent a significant health burden both locally and globally from their emissions of CO$_2$ and air toxics. The Latrobe Valley power stations constituted between 45% and 63% of Australia's mercury emissions from electricity generation, with 1,513 kg emitted in the period 2015–2016.

Several studies have shown that mercury in vegetables, grains (Li et al., 2017), cattle (Mahajan et al., 2012), and soils (Rodriguez Martin and Nanos, 2016) up to 15 km surrounding power plants are often significantly enhanced over background levels. However, the soil enhancements are highly variable between power stations, with no mercury enhancement in soils due to fly ash deposition also being observed if the mercury content of coal is extremely low (Rodriguez Martin et al., 2014).

Table 1. 2015–2016 total air pollutant emissions and associated health costs for the four major power stations in the Latrobe Valley and the electricity sector of Australia. DOI: https://doi.org/10.1525/elementa.2021.00072.t1

Air Pollutant / $A Health Costs	Loy Yang A	Loy Yang B	Hazelwood	Yallourn	Latrobe Valley	Australia
CO_2 [Mt-CO_2e][a]	19.1	10.6	15.8	16.5	61.93	201.2[b]
A_{2016}[c]	$1.14B	$629M	$932M	$974M	$3.7B	$12.0B
SO_2 (kg)[d]	6.10E+07	2.38E+07	1.69E+07	2.13E+07	1.23E+08	4.87E+08
A_{2016}[c]	$1.61B	$628M	$445M	$561M	$3.2B	$12.8B
NO_x [kg][d]	2.05E+07	1.48E+07	2.76E+07	1.52E+07	7.82E+07	3.63E+08
A_{2016}[c,e]	$504M	$365M	$679M	$374M	$1.9B	$8.9B
$PM_{2.5}$ (kg)[d]	7.20E+05	5.25E+05	6.98E+05	8.35E+05	2.77E+06	8.26E+06
A_{2016}[f]	$37M	$27M	$36M	$43M	$143M	$425M
Hg (kg)[d]	427	384	406	297	1514	2801
Hg (kg)[g]	417	231	345	360	1353	–
A_{2016}[c]	$15M	$13M	$14M	$10M	$52M	$97M
Cd (kg)[d]	47	39	40	44	170	482
A_{2016}[c]	$9.9M	$8.2M	$8.4M	$9.2M	$35.6M	$101M
Pb (kg)[d]	222	83	200	146	651	3180
A_{2016}[c]	$9.8M	$3.7M	$8.8M	$6.5M	$28.8M	$141M
As (kg)[d]	68	31	67	56	222	1303
A_{2016}[c]	$0.6M	$0.3M	$0.6M	$0.5M	$1.9M	$11M
Total costs A_{2016}	$3.33B	$1.67B	$1.12B	$1.98B	$9.08B	$34.5B

[a]CO_2 emissions for July 2015–June 2016 calculated by individual generator using the AEMO distribution data combined with carbon intensity data.

[b]Australian data for the combined electricity, gas, and water sector constituting 37.7% of Australia's total greenhouse gas emissions in 2016 from Australia's national inventory by sector 2016 report.

[c]The cost associated with each kilogram of pollutant[d] released to the air from coal combustion following Nedellec and Rabl (2016) Table VII (applying inflation adjustment of 1.8% annually to 2016 and an exchange rate of 1 EUR = 0.7 AUD).

[d]Pollutant emissions provided by the National Pollutant Inventory (www.npi.gov.au).

[e]NO_x treated identically to NO_2 for cost, in the absence of separate NO_2 pollution figures for Australia.

[f]$PM_{2.5}$ pollutant cost is taken as $AUD_{2016}51.39 per kg ($AUD_{2011}47 per kg inflation adjusted; Aust et al., 2013) for the Latrobe Valley. This cost impact is also applied to national figures as most electricity generation is away from densely populated centers.

[g]Hg derived from July 2015 to June 2016 AEMO CO_2 emissions[a] ($CO_2/44 \times 12 \times 0.08$ mgkg^{-1}).

The soil to air fluxes of mercury from mercury enhanced soils is also highly variable with light, temperature, soil moisture, precipitation, atmospheric oxidants, atmospheric background mercury concentrations, and soil substrate properties influencing fluxes (Gustin et al., 2008 and references therein). Atmospheric mercury fluxes of 15 ng m^{-2}h^{-1} were found for daytime and 5 ng m^{-2}h^{-1} for nighttime conditions when stabilized soil material was mixed with fly ash sludge to produce a mercury soil concentration enhancement of up to 1,000 μg kg^{-1} in an agricultural setting and under winter conditions (Gustin et al., 2008).

Power plants that have operated for over 30 years have been associated with extreme soil concentration enhancements up to 40,000 μg kg^{-1} compared to a background of 37 μg kg^{-1} in China (Li et al., 2017) and up to 1,400 μg kg^{-1} in Spain (Rodriguez Martin and Nanos, 2016). Similarly, in

Canada, soil concentrations surrounding a smelter were found to be extremely enhanced in mercury with 99,000 μg kg^{-1}, which 3–4 months after closure of the facility resulted in observed soil fluxes of 108 ng m^{-2}h^{-1} (Eckley et al., 2015). In Australia, Emmerson et al. (2015) conducted a modeling study of mercury emission fluxes from the Latrobe valley power stations and concluded that the perturbation to the total atmospheric mercury concentrations from the power plants to the region was <1%. However, they predicted significant local wet deposition fluxes to the soils on average 0.29 ng m^{-2}h^{-1} (maximum of 0.95 ng m^{-2}h^{-1}) and the dry deposition fluxes of 0.52 ng m^{-2}h^{-1} (maximum of 3.27 ng m^{-2}h^{-1}). The fluxes were found within 5–10 km, downwind (predominantly eastward of) and maximum closest to the power stations. This modeling was supported by observations made by Dutt et al. (2009), who observed wet deposition

mercury fluxes 10 km downwind from two black coal power stations in the Hunter Valley, New South Wales, finding a daily flux between 50 and 80 ng m^{-2}, equating to 2.0–3.3 ng m^{-2}h^{-1}. Howard and Edwards (2018) observed nocturnal deposition fluxes of 1.5 ng m^{-2}h^{-1} and daytime emission fluxes of 1.8 ng m^{-2}h^{-1} for the Australian Snowy alpine grassland region. Horowitz et al. (2017) simulated a Hg(II) deposition flux of 1–2 ng m^{-2}h^{-1} for the South-East Australian region. To our knowledge, there has been no soil assessment for mercury contamination surrounding the power stations in Australia. Similarly, to our knowledge, there has been no reported soil flux measurements in the Latrobe valley region of Victoria.

In this study, we present observations made in the coal-fired power generation Latrobe region of Victoria, Australia. In order to simulate our atmospheric mercury observations using Weather Research and Forecast model with Chemistry (WRF-Chem) modeling, we required the inclusion of soil fluxes consistent with those observed in the coal-fired power generation Hunter Valley region of New South Wales. Coal-fired power generation has long-term health implications, of which mercury is one concern, we introduce this briefly in the following section.

1.1. Health implications
Sulfur and nitrogen oxides, particles, and mercury by-products have significant health costs associated with their emissions. Electricity energy production accounted for 19% of Australia total mercury emissions in 2015–2016 (NPI data—see **Figure 1**). Cost assessments for mercury are dominated by human health costs as these are assumed to exceed those of ecosystem damage. The cost associated with each kilogram of pollutant released to the air from Australian and Latrobe Valley coal combustion is given in **Table 1** derived using the methodology described in Nedellec and Rabl (2016). Nationally, coal generation in 2016 is estimated to have had a health cost of approximately $AUD34.5B. The closure of Hazelwood in 2017 is estimated to have an annual health benefit for Victoria of approximately $AUD1.1B in 2017. The costing presented in **Table 1** are similar to those given in the Australian Academy of Technological Sciences and Engineering report (Biester et al., 2007); both the costs of the Biester et al. (2007) report and those presented in **Table 1** are based on costs derived from the EU External Costs of Energy (ExternE project—http://www.externe.info/externe_d7/) data.

To put the numbers in **Table 1** in context: Victoria's gross state product (GSP) in 2016 was $AUD 374B and Australia's gross domestic product (GDP) was $1,660B (ABS reports),[1,2] with Victoria spending $41B and Australia $170.4B on health in 2015/2016 (Australian Institute of

---

1. ABS report 5204. Available at http://www.abs.gov.au/AUSSTATS/abs@.nsf/DetailsPage/5204.02016-17?OpenDocument, Table 1. Accessed 5 March 2021.

2. ABS report 5220. Available at http://www.abs.gov.au/AUSSTATS/abs@.nsf/DetailsPage/5220.02015-16?OpenDocument Table 1. Accessed 5 March 2021.

Health and Welfare, 2017). So, the air pollution from the coal powered electricity generation in the Latrobe Valley constitutes a loss of 2.4% of the Victorian GSP, and the whole electrical sector of Australia represents a 2.1% loss of GDP nationally. In relative terms, these externalities represent 22% for Victoria and 20% for Australia of the total health expenditures, respectively.

In addition to human health costs, productivity losses due to mercury are calculated as a decrease in IQ points at a rate of 1.36 points per kilogram of mercury emitted (a cost of $US18k per IQ point, Spadaro and Rabl, 2008). This represents an additional cost of $US27M ($AUD2016 36M) from the Latrobe valley and $US50M ($AUD2016 67M) nationally using 2015–2016 NPI mercury emissions.

2. Observations
2.1. Site description
In situ observations of GEM were conducted in Churchill, Victoria, Australia (38°18′44″S, 146°25′42″E) from May 31, June 1–30, and July 1–4, 2013. The Latrobe Valley with a population of approximately 125,000 lies approximately 150 km East of Melbourne and supplies around 80% of Victoria's electricity using low-rank brown coal-fired power stations of Yallourn, Loy Yang A and B, and until March 31, 2017, Hazelwood (**Figure 2**). Observations of GEM were made from the roof on the Monash Gippsland Campus, now Federation University, in Churchill, Victoria, Australia (38°18′44″S, 146°25′42″E) from May 31, June 1–30, and July 1–4, 2013. The weather protected inlet was positioned off the northwest corner of the chemistry building roof, marked with blue star on the map given in **Figure 2**. The observation site lies 5 km to the southeast of Hazelwood power station and 15 km to the southwest of the Loy Yang A and B power stations.

Unfortunately, no colocated meteorological or concurrent chemical measurements were made with the GEM measurements at Churchill—our focus was mercury not air quality or oxidation chemistry though we note that future studies would benefit from these auxiliary observations. Meteorological observations were made at the Bureau of Meteorology (BoM) station at the Latrobe Airport indicated by the purple star in **Figure 2b**.

2.2. Sampling methods
Surface GEM measurements of air were made using a Tekran 2537. A 25-m Teflon sample line heated to 50 °C with a PTFE (teflon) particulate filter, pore size 0.2 μm, diameter 47 mm at the air intake removing for large particles was contained within a 30-cm diameter stainless steel hood for weather protection. The heated sample line ran 25 m to the Tekran instrument housed in the laboratory below. Argon (99.999% purity) was fed into the instrument via 1/8″ Teflon tubing. The filter combined with the long sample line gives us confidence that gaseous oxidized mercury (Lyman et al., 2010) and particulate mercury were excluded from our observations (similar observational set up was used by Slemr et al., 2015, for the Southern Hemispheric sites we compare with).

GEM was measured at 5-min intervals on two parallel gold traps. Although GEM was collected on one gold trap,
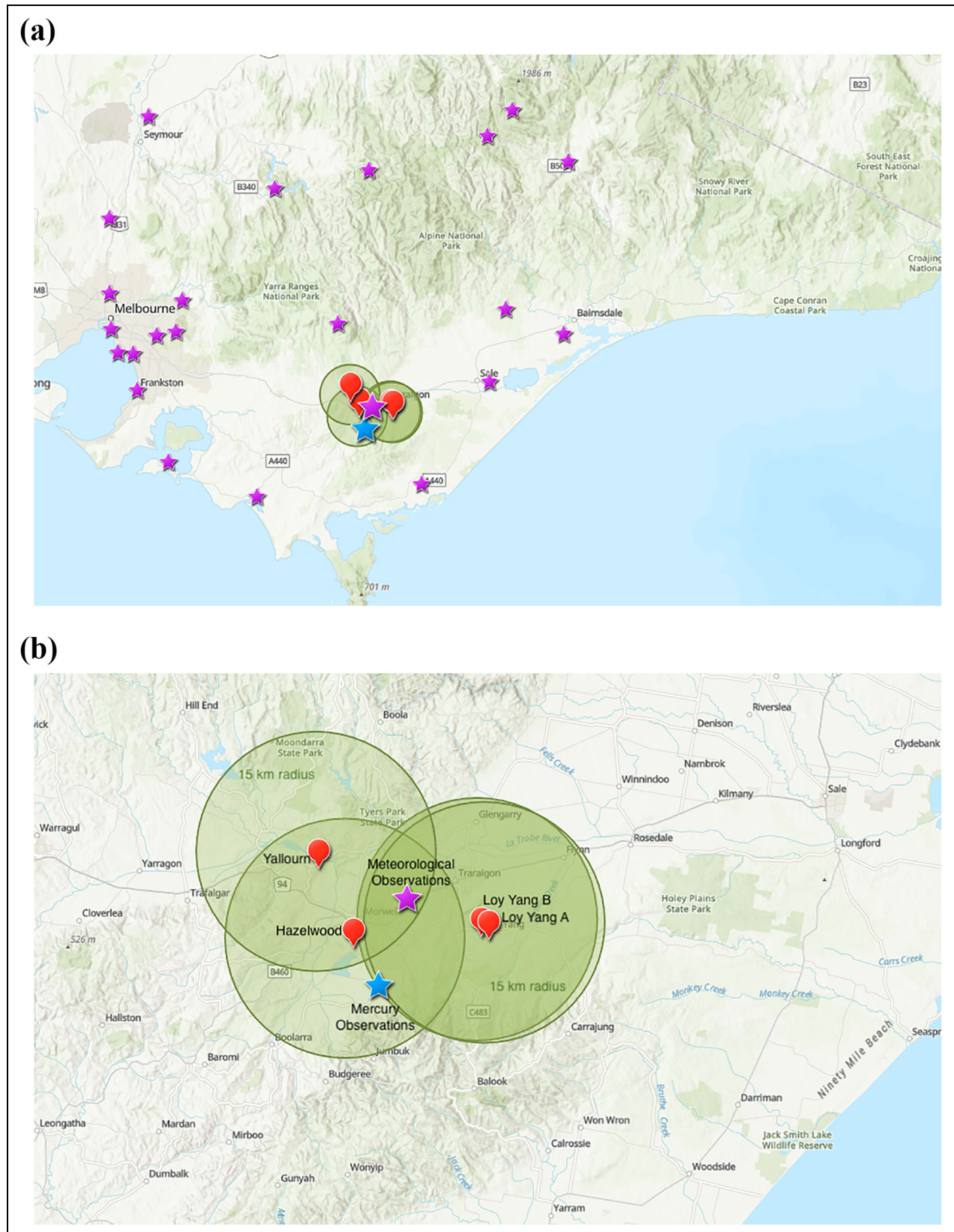
(a)

(b)

Figure 2. Topographical maps of the power stations in relation to the populations centers in the east of the State of Victoria (a) and in the Latrobe Valley (b). Melbourne has a population 4.4M, Morwell, approximately 74,000, and Churchill approximately 4,500 in 2016. The mercury observational site is shown by the blue star. The Bureau of Meteorology's stations in Eastern Victoria are given by the purple stars in (a) and the Latrobe Airport meteorology site is indicated in (b) by the larger purple star. The major power stations are given by the red pins and a 15 km radius around them by the green shading. (a) Eastern Victoria. (b) Latrobe Valley. DOI: https://doi.org/10.1525/elementa.2021.00072.f2
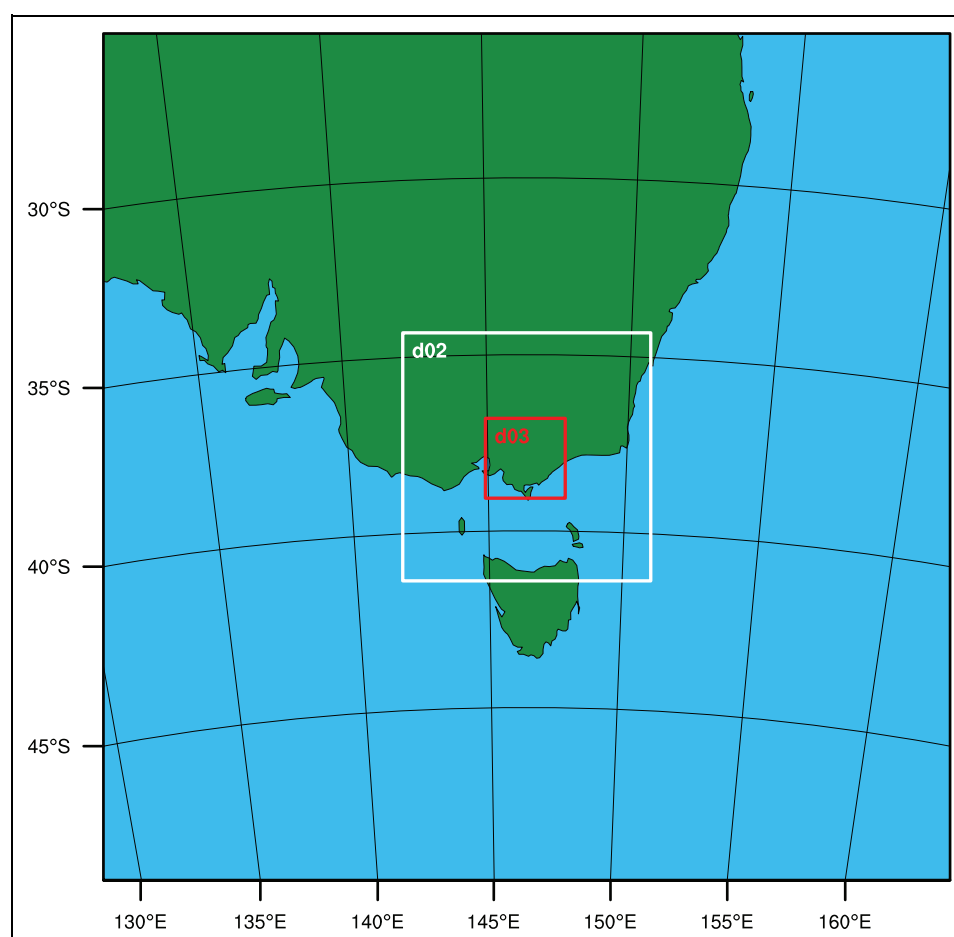
Figure 3. Three nested domain setup for runs used in this study. Horizontal resolution of 27, 9, and 3 km for outermost to innermost domains, respectively. DOI: https://doi.org/10.1525/elementa.2021.00072.f3

the GEM on the other trap was thermally desorbed and detected by a cold vapor atomic fluorescence spectrometer. The Tekran was calibrated approximately every 3–24 h using an internal mercury permeation source. The internal calibration source was checked prior to shipping the instrument to Australia using an external mercury source and verified upon return of the instrument to the USGS laboratory after deployment.

2.3. Modeling
Atmospheric modeling efforts to date have been largely influenced by knowledge of mercury in the northern hemisphere, with the exception of Nelson et al. (2011) and Emmerson et al. (2015). Recently, and with the availability of global data sets, model evaluation has improved for the Southern Hemisphere (Horowitz et al., 2017; UNEP, 2018). The WRF-Chem is used here to model the mesoscale (3 × 3 km) meteorology and GEM. WRF-Chem builds upon the advanced research WRF core meteorology with gas-phase chemistry, dry deposition, and aerosol schemes (Grell et al., 2005). For the purpose of this study, we have used version 3.7.1.

2.3.1. Model setup
The Lambert conformal projection was used to map the model grid to the surface of the Earth. As shown in **Figure 3**, our model domain setup is comprised of three nested

domains with the outermost to innermost domains at a resolution of 27, 9, and 3 km, respectively. In the vertical, the model has 30 levels with increased vertical resolution in the first few levels in the boundary layer. The model is forced at the boundaries every 6 h by ERA Interim reanalyses.

WRF-Chem has a wide selection of parameterization options representing physical processes that occur in the atmosphere (Skamarock and Klemp, 2008). We have used the Noah for the land surface model (Chen and Dudhia, 2001), the Yonsei University (YSU) Planetary Boundary Layer scheme (Hong et al., 2006), the WRF single-moment 5-class scheme Lin microphysics scheme (Lin et al., 1983), and the Rapid Radiative Transfer radiation scheme Mlawer et al. (1997). A summary of physics schemes used in the model runs is presented in **Table 2**.

The model has been run using both the tracer option and a full chemistry scheme. In the former, mercury is just advected with no chemical production or loss. For the chemistry option, we have used the extended CB05 mechanism (e.g., Karamchandani et al., 2012), which includes the oxidation of elemental mercury by O_3, OH, and H_2O_2 with the reactions and rates provided in **Table 3**.

We chose not to explore halogen chemistry here, as we have not observed evidence for halogen oxidative products. Halogen chemistry has been indicated to be

Table 2. Physics schemes used in WRF model setup for Latrobe Valley. DOI: https://doi.org/10.1525/elementa.2021.00072.t2

Type	Selected Option
Boundary layer	YSU scheme
Land surface	Noah land-surface model
Surface layer	Monin–Obukhov (Janjic Eta) scheme
Long-wave radiation	Rapid Radiative Transfer scheme
Short-wave radiation	Goddard shortwave scheme
Microphysics	WRF single-moment 5-class scheme (Lin)
Cumulus scheme	Grell 3-D ensemble scheme

WRF = Weather Research and Forecast.

Table 3. Mercury chemistry and rate constants included in the Chemistry run (Karamchandani et al., 2012). DOI: https://doi.org/10.1525/elementa.2021.00072.t3

Equation No.	Reaction	Rate Constant
1	$Hg^0 + O_3 \rightarrow Hg^{2+}$	3.0×10^{-20}
2	$Hg^0 + OH \rightarrow Hg^{2+}$	8.7×10^{-14}
3	$Hg^0 + H_2O_2 \rightarrow Hg^{2+}$	8.5×10^{-19}

important in mercury oxidation, in particular chlorine in forming particulate mercury in coal combustion (Dutt et al., 2009), marine or dramatic springtime, polar bromine explosion/mercury depletion events (i.e., Steffen et al., 2008), and recent modeling studies of free tropospheric bromine–driven mercury oxidation (Wang et al., 2015). Recent aircraft observations support a free tropospheric bromine budget of 2 pptv in the tropical western pacific (Koenig et al., 2017). However, as noted by Theys et al. (2011), there remains a discrepancy between satellite-derived tropospheric columns, which are challenged to separate the stratospheric and tropospheric columns (Salawitch et al., 2010) and ground-based/balloon measurements. Ground-based observations in the Southern Hemisphere, that is, for Lauder (Schofield et al., 2004), balloon observations (Dorf et al., 2008), and our recent MAX-DOAS observations made in Melbourne 2016–2020 have not observed a tropospheric BrO column >0.5 pptv (Ryan et al., 2020). Further ground-based and satellite validation of halogen observations over Australia are required to constrain the importance of halogen mercury oxidation as postulated by the mercury modeling of Wang et al. (2015).

2.4. Emissions
For the mercury emissions, both the Edgar v4.3.1 gridded emissions 0.1 × 0.1 (11 × 11 km) last updated in 2008 for Australia were initially used (Crippa et al., 2016) along with a calculation of the emissions from the four large

power stations based on their power output and emissions intensity data. We found for the Edgar dataset that the point sources had erroneous geolocations and also were deficient in their temporal resolution (simply an annual value), thus providing spatially and temporally deficient results. Instead, using the accurate locations of the power stations combined with their 30-min electricity dispatch data multiplied by the carbon intensity (Hazelwood: 1.53 tCO$_2$/MWh, Yallourn: 1.42, Loy Yang A: 1.21, Loy Yang B: 1.24, AEMO, 2019) and assuming an emission of 0.032-mg mercury for each kilogram of wet coal burnt (0.08-mg mercury for each kilogram of dry coal), which is typical for Australian brown coal (Nelson, 2007), gave high-resolution point source mercury emissions for the power stations in the Latrobe Valley. Primary measures to remove mercury such as coal washing, blending, or additives and postcombustion measures such as from electrostatic precipitators (which is largely untested or only 1%–2% efficient for lignite, Pacyna et al., 2010) are assumed to be captured within the 50% uncertainty in the 0.08 mg kg^{-1} of the carbon emission factor we use here (Nelson, 2007). In the absence of stack measurements of mercury emissions, we cannot know the efficiency of mercury removal from primary and postcombustion measures, but to first order mercury emissions are a function of the quantity of coal burnt (Pacyna et al., 2010). The NPI provides industry reported annual mercury emissions; these are given in **Table 1** alongside those we have calculated from 30-min AEMO generation for 2015–2016 using published 0.08-mg kg^{-1} mercury to carbon emission factor. The variability between the industry reported and energy production–derived mercury emissions indicates significant differences that routine stack measurements would help resolve (the NPI values representing underestimates of 21% to overestimates of 40%, which are within the 50% uncertainty range but represent a discrepancy of several million dollars in health cost externalities estimates).

Time series of the emission fluxes that were used in the model run are shown in **Figure 4**. A map showing the locations of the power stations and the measurement sites in the Latrobe Valley is shown in **Figure 2**.

3. Results and discussion
The observed GEM values at Churchill displayed in **Figures 5−7** show a strong diurnal variation. Observations were conducted from late May to early July, late autumn to early winter, typically a time of the year in Victoria, Australia, in which strong nocturnal boundary layer inversions are experienced. Overnight (6 PM–6 AM), the observed mercury averages ranged from 1.6 to 1.8 ng m^{-3}, and during the day (6 a.m.–6 p.m.), an average of 1.2–1.3 ng m^{-3} was observed (**Figure 5**). These average observed values are significantly higher than the annual averages reported for Cape Grim of 0.85–0.96 ng m^{-3} and the Southern Hemisphere monitoring stations of 0.85–1.05 ng m^{-3} for the 2007–2013 period (Slemr et al., 2015). This indicates that the atmospheric Total Gaseous Mercury (TGM) in the Latrobe valley is elevated, perhaps
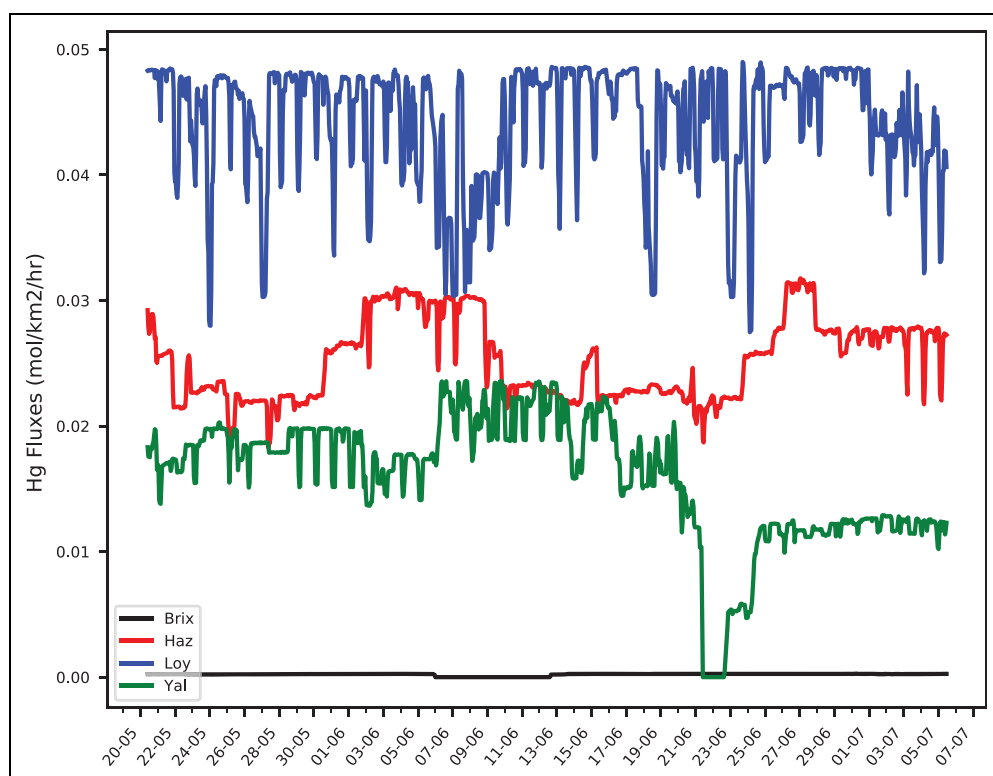
Figure 4. Time series of gaseous elemental mercury emission fluxes from power stations used in the model. DOI: https://doi.org/10.1525/elementa.2021.00072.f4
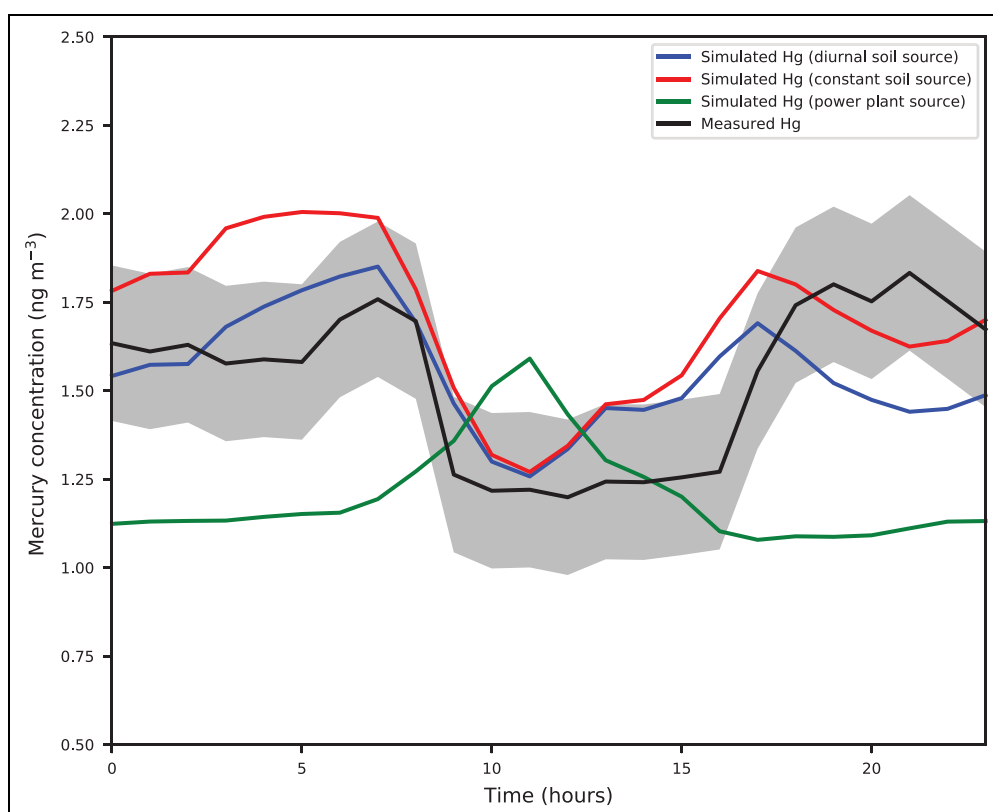
Figure 5. Measured (black), with 1 standard deviation (gray shading) and simulated diurnally averaged gaseous elemental mercury concentrations using a constant soil (red), diurnally varying soil (blue) and power plant only (green) sources. DOI: https://doi.org/10.1525/elementa.2021.00072.f5
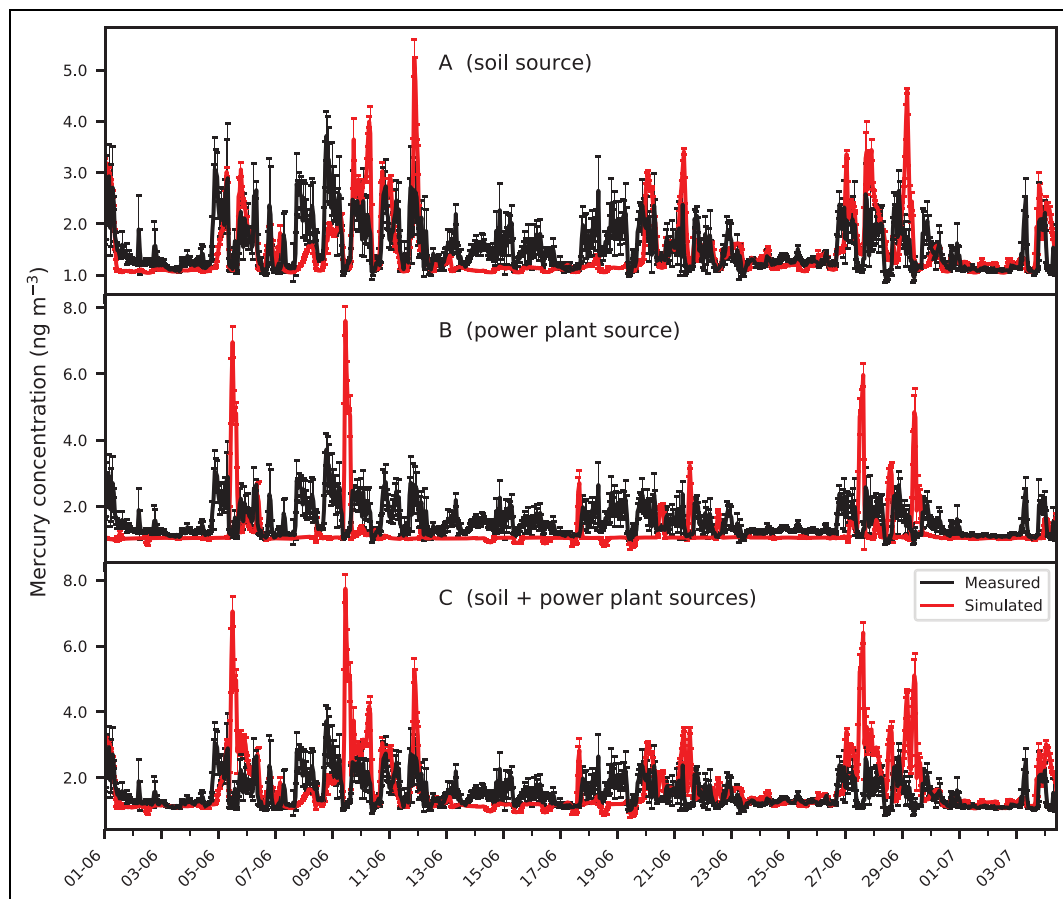
Figure 6. Time series of hourly averaged measured (black) and simulated (red) gaseous elemental mercury using soil source (A), power plant source (B), and both sources (C). DOI: https://doi.org/10.1525/elementa.2021.00072.f6
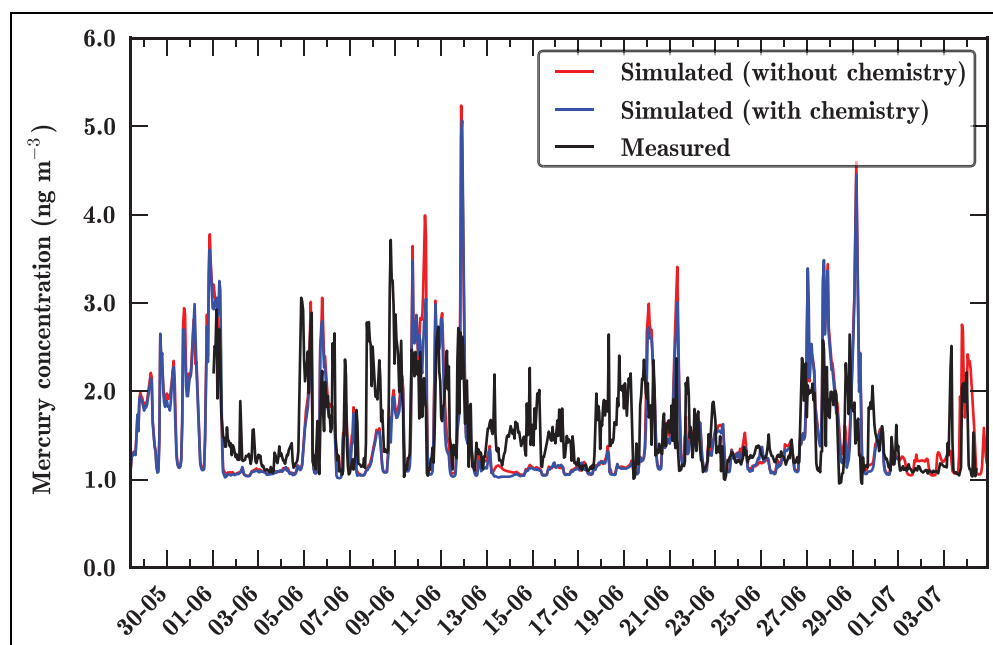
Figure 7. A comparison of measured (black) and simulated gaseous elemental mercury (red) time series (simulated with [blue] and without [red] chemistry). DOI: https://doi.org/10.1525/elementa.2021.00072.f7

up to 50%, relative to the background concentrations expected in the Southern Hemisphere, this is much more than the 1% predicted by Emmerson et al. (2015).

3.1. Simulation of meteorology
Accurate simulation of meteorology is critical to simulation of species with long lifetimes such as GEM. This is

Table 4. Comparison of Weather Research and Forecast model and Bureau of Meteorology (BoM) operational meteorology for the Gippsland region during June 2013. DOI: https://doi.org/10.1525/elementa.2021.00072.t4

BoM Site	R^2 (Temperature)	R^2 (Wind Speed)	R^2 (Wind Direction)
MOUNT BULLER	.77	.84	.75
FALLS CREEK	.77	.53	.42
MOUNT HOTHAM	.66	.36	.58
OMEO	.87	.69	.51
EAST SALE AIRPORT	.91	.63	.39
POUND CREEK	.91	.71	.59
YARRAM AIRPORT	.93	.75	.62
BAIRNSDALE AIRPORT	.89	.63	.38
MORWELL LATROBE VALLEY AIRPORT	.92	.60	.64
MOUNT BAW BAW	.75	.64	.74
MOUNT MOORNAPA	.78	.56	.60
VIEWBANK ARPANSA	.89	.73	.20
MOORABBIN AIRPORT	.93	.77	.65
SCORESBY RESEARCH INSTITUTE	.92	.75	.33
ST KILDA HARBOUR-RMYS	NA	.82	.37
FERNY CREEK	.81	.46	.51
CERBERUS	.92	.76	.73
FRANKSTON AWS	.86	.68	.29
RHYLL	.87	.68	.71
FAWKNER BEACON	NA	.77	62
COLDSTREAM	.92	.72	.21
MANGALORE AIRPORT	.92	.65	.13
WALLAN KILMORE GAP	.82	.83	.21
EILDON FIRE TOWER	.86	.53	.66
Average	.85	.67	.49

The site locations are indicated in **Figure 2a** for reference.

especially important for a region with complex topography such as the Latrobe Valley as shown in **Figure 2**. Therefore, it is instructive to compare how the model is simulating the observed meteorology in the Gippsland region in June 2013. We compare the model's simulation of wind speed and direction with observations from a network of meteorological measurements as part from the Australian BoM. Within the model's inner domain, there are 24 BoM sites. **Table 4** shows the R^2 correlation coefficients for simulated and measured temperature, wind speed, and wind direction. The model tends to do poorly for mountainous sites (e.g., Mount Buller, Mount Hotham, Mount Baw Baw, and Mount Mornapa) with R^2 correlation coefficient ranging from .66 (P value of 1.80E-103) to .77 (P value of 6.86E-164). In general, the simulated temperature shown in Figure 8 agrees well with the observations with an average R^2 correlation coefficient of .85 (P value of 8.22E-105). The model

simulates the observed wind speed with R^2 values ranging from .36 (P value of 2.41E-26) at Mount Hotham to maximum of .84 (P value of 2.18E-218) at Mount Buller with an average R^2 value of .67 (P value of 1.00E-27). The nearest BoM site to the mercury observational site is at Morwell (Latrobe Valley Airport), which has an R^2 value of .60 (P value of 2.02E-79). For wind direction, the R^2 values are poorer, with an average R^2 value of .49 (P value of 7.81E-08), but this is more likely due to the discontinuity between 0° and 360°, making a visual inspection more appropriate. Visually, the simulated wind direction is shown in **Figure 9** for the Morwell site, so that we can be confident that the model's simulation of the meteorology in the Latrobe Valley is reasonable, although there is a positive mean bias in simulated wind speeds at the Morwell site. On the whole, the model is simulating the observed meteorology with reasonable skill. The high R^2 value, combined with low P value, indicates the model
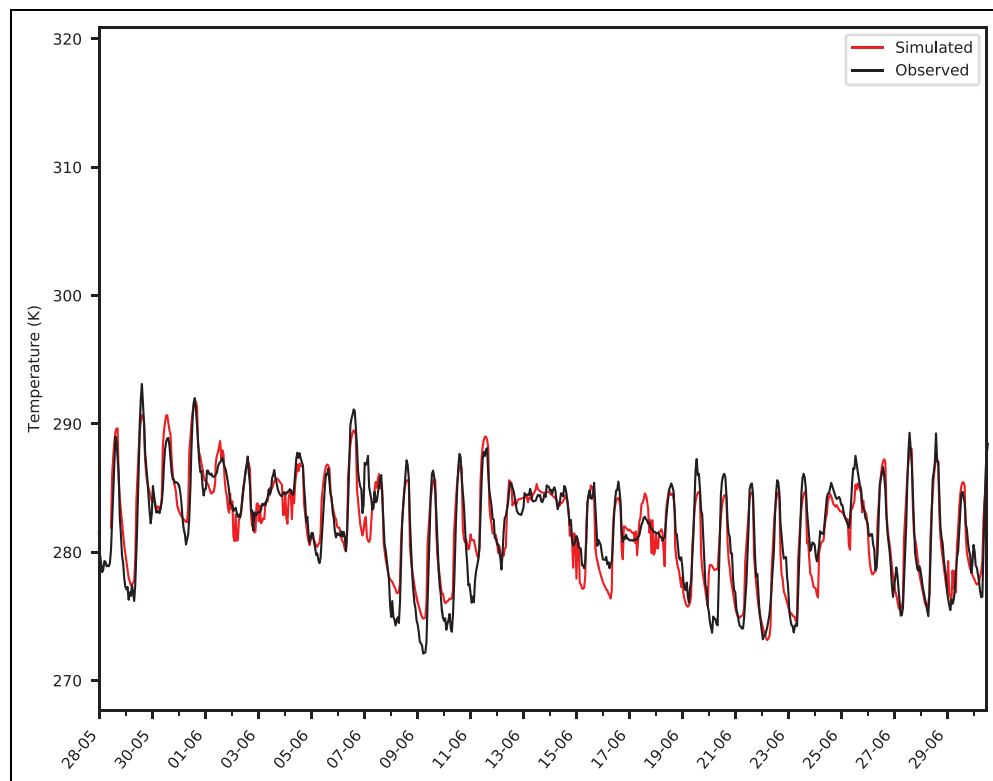
Figure 8. Time series of measured and simulated temperature at the Morwell meteorological observation site. DOI: https://doi.org/10.1525/elementa.2021.00072.f8

explains the observed variability well with significant agreement. This is obviously important for accurate simulation of observed mercury as presented in the next section.

3.2. Simulation of Mercury

Figure 6 shows the time series of hourly averaged mercury concentrations observed and for the modeled constant soil source, modeled power plant source, and the sum of the two sources. Mercury in the model is advected as a tracer (no chemistry). The soil source simulates the observed mercury concentrations better (R^2 value of .49, P value of 0.000) than the power plant source (R^2 value of $-.16$, P value of 0.000), and summation of both (R^2 value of .28, P value of 0.000). Periods of elevated mercury concentrations are generally well represented by the soil source (R^2 and P values showing significance and capturing of the variability well), although there are other times when the model does not predict the observed elevated concentrations well. These values showed that although the modeling of the power plant source had significance, it was unable to explain the observational variability. The mismatches in the magnitude and timing of the peaks and troughs in the hourly averaged concentrations between the soil + powerplant simulation and the observations are more likely attributable to model coarse spatial and/or temporal resolution compared to observations made at a single site.

It is interesting to note that there is a period of South to South-Westerly winds seen between June 13 and 19 in **Figure 6**. This is a region where there are no mercury

emissions from the power station point sources, and beyond 15 km radius from the power stations, there is no soil reemission in the model simulations. As there is still a slight diurnal cycle in the observations, it implies that the extent of soil contamination from wet/dry deposition from the power stations is beyond 15 km or that other soil contamination sources such as legacy mercury from the Gold mining period exist.

The measured and simulated diurnally averaged mercury concentrations (**Figure 5**) show a clear diurnal cycle. To some extent, this is indicative of constant or near constant source emitting into a boundary layer. The boundary layer has a strong diurnal variation, typical of early winter stability. Indeed, when we applied a constant soil source it resulted in diurnally varying concentrations due to the daily expansion and contraction of the boundary layer height, and we saw better correlations with the observations. This indicates it is the boundary layer meteorology dominating over the soil emission source strength that is driving the diurnal mercury cycling observed. The peak mercury atmospheric GEM concentrations are seen when the boundary layer is shallowest during the night (350 m) and the lowest concentrations correspond to the boundary layer breakdown during the day (daytime boundary layer depth was 800 m).

Clearly, as seen in **Figures 5** and **6b**, the model is unable to simulate this diurnal cycle using the power station emissions that peak during the day, just after sunrise, after increased mixing from aloft, and increased daytime winds bring the emissions from the power stations to the measurement site. Thus, it appears that the observed
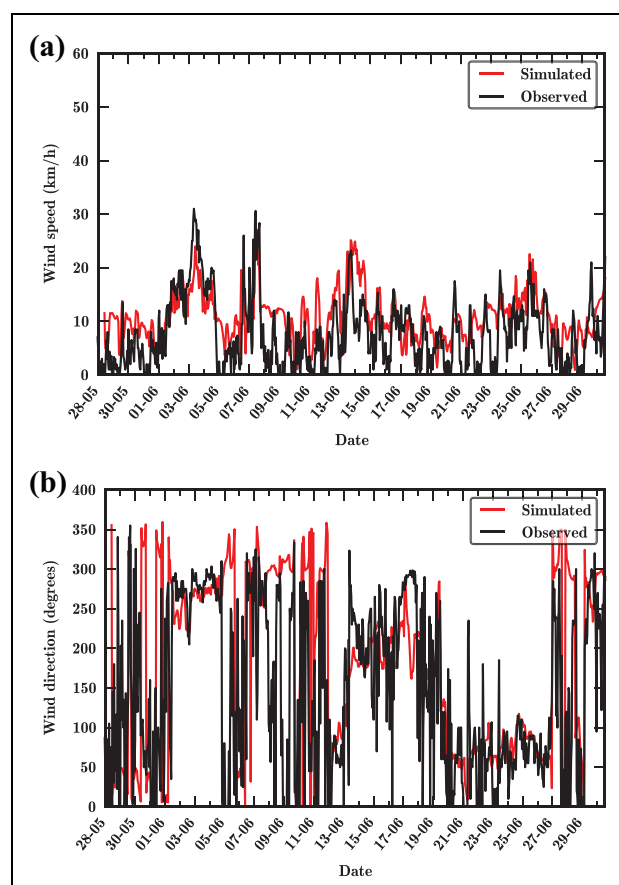
Figure 9. Time series of measured and simulated wind speed (a) and wind direction (b) at the Morwell meteorological observation site. (a) Wind speed. (b) Wind direction. DOI: https://doi.org/10.1525/elementa.2021.00072.f9

mercury concentrations as measured at the Churchill site are not directly related to the power station mercury source but most likely indirectly via soil (as only a relatively constant soil emission will provide this diurnal variation). As discussed in the Introduction section, soil is often contaminated with mercury from fly ash and wet and dry deposition within 15 km of power stations, particularly if they have been operating for 30 years or more, as is the case here. In the model setup, both Hazelwood (5 km from the observations) and Loy Yang A and B (15 km from the observations) are assumed to have deposited fly ash in a linear decreasing fashion. Soil reemissions at the power stations are assumed to be 15 ng m^{-2}h^{-1} consistent with (Gustin et al., 2008) assuming peak soil concentrations of approximately 1,000 μg kg^{-1} at the power stations, decreasing to zero at a radius of 15 km, as indicated by the green shading in **Figure 2**. Soil contamination of approximately 1,000 μg kg^{-1} is at the lower end of the range found around power stations in Spain and China (Rodriguez Martin and Nanos, 2016; Li et al., 2017). This level of reemission flux from the soil is commensurate with the wet deposition flux measured at a distance of 10 km from power stations in the Hunter Valley a mean of 3.3 ng m^{-2}h^{-1}, and a range of 0.7–10.9 ng m^{-2}h^{-1} (Dutt et al., 2009). Given that a constant emission soil source gives

us the best agreement with observations, we conclude that there is legacy build up from wet and dry deposition in a radius around the coal-fired power stations in the Latrobe valley. This is supported by the earlier modeling study of Emmerson et al. (2015) who predicted wet and dry depositions of up to 4 ng m^{-2}h^{-1} within 5–10 km of the Latrobe valley power stations. We suggest that the TGM we observed poses a greater than 1% elevation above background and that future modeling incorporates a reemission flux from the soil. The proportion of legacy mercury build up in the soil, versus daily wet/dry deposition to the soil, needs to be observationally determined to ascertain the risk posed to the local communities, water and air.

A comparison between a diurnally varying soil source and a constant soil (**Figure 5**) is inconclusive. Although both capture higher nighttime concentrations and lower daytime concentrations, neither agrees with the observations within 1 standard deviation for both morning and evening periods. This indicates that further observations of both the level of soil contamination and the diurnal fluxes that they produce are required to advance our simulation skill.

Introducing chemistry to the simulated mercury through the oxidation by O$_3$, OH and H$_2$O$_2$ makes a negligible change to the simulated mercury concentrations. **Figure 7** shows the sensitivity study comparison of measured and simulated mercury with and without chemistry (using soil source). There is a slight reduction in simulated mercury concentrations as expected but no major improvement in the correlation coefficient.

We conclude from our simulation results that the contaminated soil source, and not direct power plant sources, best describes the observed mercury profile as measured at the Churchill site in 2013.

4. Conclusions

Mercury observations in the Latrobe Valley display a strong diurnal variation, with average values approximately 50% higher than Southern Hemisphere averages for June (Slemr et al., 2015). Our work has shown that it is likely that the elevated nighttime of 1.6–1.8 ng m^{-3} average concentrations of mercury observed at the Churchill site during the spring of 2013 are dominated by mercury reemissions from the soils, into a very stable nocturnal boundary layer. Without soil testing and attribution, the source of the mercury cannot be certain. However, it has been shown that high soil mercury concentrations are found in radii up to 15 km surrounding aging coal-fired generators (Rodriguez Martin and Nanos, 2016) and wet deposition fluxes in the Hunter Valley (Dutt et al., 2009), and we hypothesize that this is the case for the Latrobe valley. Only with the inclusion of high-mercury soil emissions, decreasing from 15 ng m^{-2}h^{-1} at each power station to 0 at a 15 km radius, were we able to reconcile the temporal variation of our observations of GEM with our WRF-Chem simulations.

Future work to understand and reduce mercury in the Latrobe region requires further observation, and we strongly advise establishing longer term air and soil monitoring of mercury in the region colocated with

meteorological, including boundary layer height, and chemical observations, that is, ozone, halogens, and particles. The health benefits of reducing mercury for the region are significant at AUD_{2016}88M per year, aside from the benefits under the Minamata convention of reducing this global pollutant.

Lignite coals, such as the brown coals in Victoria, are inefficient in the conversion of carbon to electricity as significant coal is required to be burnt to dry the coal. For lignites, electrostatic precipitators or spray dryer absorber/fabric filters are only 1%–2% efficient at removing mercury postcombustion (Pacyna et al., 2010). In contrast, the bituminous coal's (in New South Wales and Queensland) mercury can be controlled by electrostatic precipitators with 14%–36% efficiency or by fabric filters by up to 90% efficiency (Pacyna et al., 2010). This may explain why our mercury observations indicate a strong diurnal variation, pointing to a contaminated soil source, that is only seen in the New South Wales coal generation regions when a stable nocturnal boundary layer is present (P Nelson, personal communication). Given the wet deposition fluxes observed by Dutt et al. (2009), we would expect similar reemission soil fluxes to be a possibility in the Hunter valley region also.

In order to reduce stack emissions of mercury for the Latrobe operators, there are clear next steps. Establishing the primary coal mercury composition and the mercury stack emissions will enable the emission factors to be more accurately established. This will aid with determining whether primary (such as washing or blending) or rather postcombustion controls of mercury would be most beneficial to the Latrobe Valley power generators. In addition, any measure to improve lignite efficiencies (such as noncombustion predrying of the coal) will have direct and immediate benefits in reducing mercury (alongside carbon, NO_x, SO_x, and particle) emissions from coal electricity generation in Victoria.

Data accessibility statement
The mercury observational data set is provided in the Supplementary Material. The Weather Research and Forecast model with Chemistry model output will be made available upon request to the authors.

Supplemental files
The supplemental files for this article can be found as follows:

'QC_NOCal_Tekran_AllData.txt' provides all the observed Tekran 2537 data (quality controlled—without calibration lines) used in the analysis presented in the main paper.

'Tekran_Raw_Files.zip' provides the raw data Tekran 2537 data as text files (daily files with full calibration details).

In situ observations of gaseous elemental mercury were conducted in Churchill, Victoria, Australia (38°18′44″S, 146°25′42″E) from May 31, June 1–30, and July 1–4, 2013.

The text files contain 13 columns: The metadata descriptions for these data, their formats and their units, and their associated headers are provided in Table 5.

Competing interests
The authors have no competing interests to declare.

Author contributions
Conceived the study and performed the data analysis: RS, RD, SU.

Contributed to conducting the mercury measurements: CG, MT, DK, RS, MK, SA.

Provided the energy data and concept: RD, MS.

Approved and submitted the version for publication: RS.

All authors contributed to the writing.

References
AEMO. 2019. Carbon dioxide equivalent intensity index procedures. Available at https://www.aemo.com.au/Electricity/National-Electricity-Market-NEM/Settlements-and-payments/Settlements/Carbon-Dioxide-Equivalent-Intensity-Index.

Amos, HM, Jacob, DJ, Streets, DG, Sunderland, EM. 2013. Legacy impacts of all-time anthropogenic emissions on the global mercury cycle. *Global Biogeochemical Cycles* **27**: 410–421. DOI: https://doi.org/10.1002/gbc.20040.

Aust, N, Watkiss, P, Boulter, P, Bawden, K. 2013. Methodology for valuing the health impacts of changes in particle emissions—Final report. Technical Report. Gladstone.

Australian Institute of Health and Welfare. 2017. Health expenditure Australia 2015–2016, 58. Canberra, Australia: AIHW.

Bieser, J, Angot, H, Slemr, F, Martin, L. 2020. Atmospheric mercury in the Southern Hemisphere – Part 2: Source apportionment analysis at Cape Point station, South Africa. *Atmospheric Chemistry and Physics* **20**(17): 10427–10439. DOI: https://doi.org/10.5194/acp-2020-63, 2020.

Biester, H, Bindler, R, Martinez-Cortizas, A, Engstrom, DR. 2007. Modeling the past atmospheric deposition of mercury using natural archives. *Environmental Science & Technology* **41**: 4851–4860.

Brunke, E-G, Walters, C, Mkololo, T, Martin, L, Labuschagne, C, Silwana, B, Slemr, F, Weigelt, A, Ebinghaus, R, Somerset, V. 2016. Mercury in the atmosphere and in rainwater at Cape Point, South Africa. *Atmospheric Environment* **125**: 24–32.

Chen, F, Dudhia, J. Coupling an advanced land surface-hydrology model with the Penn state-NCAR MM5 modeling system. Part 1: Model implementation and sensitivity. *Monthly Weather Review* **129**: 569–585.

Crippa, M, Janssens-Maenhout, G, Dentener, F, Guizzardi, D, Sindelarova, K, Muntean, M, Van Dingenen, R, Granier, C. 2016. Forty years of improvements in European air quality: regional policy-industry interactions with global impacts. *Atmospheric Chemistry and Physics* **16**: 3825–3841.

Dommergue, A, Sprovieri, F, Pirrone, N, Ebinghaus, R, Brooks, S, Courteaud, J, Ferrari, CP. 2010. Overview of mercury measurements in the Antarctic troposphere. *Atmospheric Chemistry and Physics* **10**: 3309–3319.

Dorf, M, Butz, A, Camy-Peyret, C, Chipperfield, MP, Kritten, L, Pfeilsticker, K. 2008. Bromine in the tropical troposphere and stratosphere as derived from balloon-borne BrO observations. *Atmospheric Chemistry and Physics* **8**: 7265–7271.

Dutt, U, Nelson, PF, Morrison, AL, Strezov, V. 2009. Mercury wet deposition and coal-fired power station contributions: an Australian study. *Fuel Processing Technology* **90**: 1354–1359.

Eckley, CS, Blanchard, P, McLennan, D, Mintz, R, Sekela, M. 2015. Soil-Air Mercury Flux near a Large Industrial Emission Source before and after Closure (Flin Flon, Manitoba, Canada). *Environmental Science and Technology* **49**: 9750–9757. DOI: https://doi.org/10.1021/acs.est.5b01995.

Emmerson, K, Cope, M, Lee, S, Hibberd, M, Torre, P. 2015. Modelling atmospheric mercury from power stations in the Latrobe Valley, Victoria. *Air Quality and Climate Change* **49**: 33.

Grell, GA, Peckham, SE, Schmitz, R, McKeen, SA, Frost, G, Skamarock, WC, Eder, B. 2005. Fully coupled "online" chemistry within the WRF model. *Atmospheric Environment* **39**: 6957–6975.

Gustin, MS, Ericksen, J, Fernandez, GC. 2008. Determination of the potential for release of mercury from combustion product amended soils: Part 1—Simulations of beneficial use. *Journal of the Air & Waste Management Association* **58**: 673–683.

Hong, S-Y, Noh, Y, Dudhia, J. 2006. A new vertical diffusion package with an explicit treatment of entrainment processes. *Monthly Weather Review* **134**: 2318–2341. DOI: https://doi.org/10.1175/MWR3199.

Horowitz, HM, Jacob, DJ, Zhang, Y, DIbble, TS, Slemr, F, Amos, HM, Schmidt, JA, Corbitt, ES, Marais, EA, Sunderland, EM. 2017. A new mechanism for atmospheric mercury redox chemistry: Implications for the global mercury budget. *Atmospheric Chemistry and Physics* **17**: 6353–6371. DOI: https://doi.org/10.5194/acp-17-6353-2017.

Howard, D, Edwards, GC. 2018. Mercury fluxes over an Australian alpine grassland and observation of nocturnal atmospheric mercury depletion events. *Atmospheric Chemistry and Physics* **18**: 129–142. DOI: https://doi.org/10.5194/acp-18-129-2018.

Howard, D, Macsween, K, Edwards, GC, Desservettaz, M, Guérette, EA, Paton-Walsh, C, Surawski, NC, Sullivan, AL, Weston, C, Volkova, L, Powell, J, Keywood, MD, Reisen, F, Meyer, CP. 2019. Investigation of mercury emissions from burning of Australian eucalypt forest surface fuels using a combustion wind tunnel and field observations. *Atmospheric Environment* **202**: 17–27. DOI: https://doi.org/10.1016/j.atmosenv.2018.12.015.

Howard, D, Nelson, PF, Edwards, GC, Morrison, AL, Fisher, JA, Ward, J, Harnwell, J, van der Schoot, M, Atkinson, B, Chambers, SD, Griffiths, AD, Werczynski, S, Williams, AG. 2017. Atmospheric mercury in the Southern Hemisphere tropics: seasonal and diurnal variations and influence of interhemispheric transport. *Atmospheric Chemistry and Physics* **17**: 11623–11636.

Karamchandani, P, Zhang, Y, Chen, S, Balmori-Bronson, R. 2012. Development of an extended chemical mechanism for global-through-urban applications. *Atmospheric Pollution Research* 3: 1–24. DOI: https://doi.org/10.5094/APR.2011.047.

Koenig, TK, Volkamer, R, Baidar, S, Dix, B, Wang, S, Anderson, DC, Salawitch, RJ, Wales, PA, Cuevas, CA, Fernandez, RP, Saiz-Lopez, A, Evans, MJ, Sherwen, T, Jacob, DJ, Schmidt, J, Kinnison, D, Lamarque, JF, Apel, EC, Bresch, JC, Campos, T, Flocke, FM, Hall, SR, Honomichl, SB, Hornbrook, R, Jensen, JB, Lueb, R, Montzka, DD, Pan, LL, Michael Reeves, J, Schauffler, SM, Ullmann, K, Weinheimer, AJ, Atlas, EL, Donets, V, Navarro, MA, Riemer, D, Blake, NJ, Chen, D, Gregory Huey, L, Tanner, DJ, Hanisco, TF, Wolfe, GM. 2017. BrO and inferred Bry profiles over the western Pacific: Relevance of inorganic bromine sources and a Bry minimum in the aged tropical tropopause layer. *Atmospheric Chemistry and Physics* **17**: 15245–15270. DOI: https://doi.org/10.5194/acp-17-15245-2017.

Li, R, Wu, H, Ding, J, Fu, W, Gan, L, Li, Y. 2017. Mercury pollution in vegetables, grains and soils from areas surrounding coal-fired power plants. *Scientific Reports* **7**(1): 1–9.

Lin, Y-L, Farley, RD, Orville, HD. 1983. Bulk parameterization of the snow field in a cloud model. *Journal of Climate and Applied Meteorology* **22**: 1065–1092.

Lyman, SN, Gustin, MS, Prestbo, EM. 2010. A passive sampler for ambient gaseous oxidized mercury concentrations. *Atmospheric Environment* **44**: 246–252. DOI: https://doi.org/10.1016/j.atmosenv.2009.10.008.

Mahajan, VE, Yadav, RR, Dakshinkar, NP, Dhoot, VM, Bhojane, GR, Naik, MK, Shrivastava, P, Naoghare, PK, Krishnamurthi, K. 2012. Influence of mercury from fly ash on cattle reared nearby thermal power plant. *Environmental Monitoring and Assessment* **184**: 7365–7372.

Martin, LG, Labuschagne, C, Brunke, EG, Weigelt, A, Ebinghaus, R, Slemr, F. 2017. Trend of atmospheric mercury concentrations at Cape Point for 1995–2004 and since 2007. *Atmospheric Chemistry and Physics* **17**: 2393–2399. DOI: https://doi.org/10.5194/acp-17-2393-2017.

Mlawer, EJ, Taubman, SJ, Brown, PD, Iacono, MJ, Clough, SA. 1997. Radiative transfer for inhomogeneous atmospheres: RRTM, a validated correlated-k model for the longwave. *Journal of Geophysical Research: Atmospheres* **102**: 16663–16682. DOI: https://doi.org/10.1029/97JD00237.

Nedellec, V, Rabl, A. 2016. Costs of health damage from atmospheric emissions of toxic metals: Part 1-Methods and results. *Risk Analysis* **36**: 2081–2095.

Nelson, PF. 2007. Atmospheric emissions of mercury from Australian point sources. *Atmospheric Environment* **41**: 1717–1724.

Nelson, PF, Nguyen, H, Morrison, AL, Cope, ME, Hibberd, MF, Lee, S, McGregor, JL, Meyer, M. 2011. Mercury Sources, Transportation and Fate in Australia. Technical Report. Canberra, Australia: RFT 100/0607.

Outridge, PM, Mason, RP, Wang, F, Guerrero, S, Heimbürger-Boavida, LE. 2018. Updated global and oceanic mercury budgets for the United Nations Global Mercury Assessment 2018. *Environmental Science and Technology* **52**: 11466–11477. DOI: https://doi.org/10.1021/acs.est.8b01246.

Pacyna, JM, Sundseth, K, Pacyna, EG, Jozewicz, W, Munthe, J, Belhaj, M, Aström, S. 2010. An assessment of costs and benefits associated with mercury emission reductions from major anthropogenic sources. *Journal of the Air & Waste Management Association* **60**: 302–315.

Rodriguez Martin, JA, Nanos, N. 2016. Soil as an archive of coal-fired power plant mercury deposition. *Journal of Hazardous Materials* **308**: 131–138.

Rodriguez Martin, JA, Nanos, N, Grigoratos, T, Carbonell, G, Samara, C. 2014. Local deposition of mercury in topsoils around coal-fired power plants: is it always true? *Environmental Science and Pollution Research* **21**: 10205–10214.

Ryan, R, Silver, J, Querel, R, Smale, D, Rhodes, S, Tully, M, Jones, N, Schofield, R. 2020. Comparison of formaldehyde tropospheric columns in Australia and New Zealand using MAX-DOAS, FTIR and TROPOMI, accepted. *Atmospheric Measurement Techniques* **13**(12): 1–28. DOI: https://doi.org/10.5194/amt-2020-232.

Salawitch, RJ, Canty, T, Kurosu, T, Chance, K, Liang, Q, da Silva, A, Pawson, S, Nielsen, JE, Rodriguez, JM, Bhartia, PK, Liu, X, Huey, LG, Liao, J, Stickel, RE, Tanner, DJ, Dibb, JE, Simpson, WR, Donohoue, D, Weinheimer, A, Flocke, F, Knapp, D, Montzka, D, Neuman, JA, Nowak, JB, Ryerson, TB, Oltmans, S, Blake, DR, Atlas, EL, Kinnison, DE, Tilmes, S, Pan, LL, Hendrick, F, Van Roozendael, M, Kreher, K, Johnston, PV, Gao, RS, Johnson, B, Bui, TP, Chen, G, Pierce, RB, Crawford, JH,

Jacob, DJ. 2010. A new interpretation of total column BrO during Arctic spring. *Geophysical Research Letters* **37**(21): 1–9.

Schofield, R, Kreher, K, Connor, B, Johnston, P, Thomas, A, Shooter, D, Chipperfield, M, Rodgers, C, Mount, G. 2004. Retrieved tropospheric and stratospheric BrO columns over Lauder, New Zealand. *Journal of Geophysical Research* **109**. DOI: https://doi.org/10.1029/2003JD004 463.

Selin, NE, Jacob, DJ, Park, RJ, Yantosca, RM, Strode, S, Jaegle, L, Jaffe, D. 2007. Chemical cycling and deposition of atmospheric mercury: Global constraints from observations. *Journal of Geophysical Research-Atmospheres* **112**(D2): 1–14.

Skamarock, WC, Klemp, JB. 2008. A time-split nonhydrostatic atmospheric model for weather research and forecasting applications. *Journal of Computational Physics* **227**: 3465–3485. DOI: https://doi.org/10.1016/j.jcp.2007.01.037.

Slemr, F, Angot, H, Dommergue, A, Magand, O, Barret, M, Weigelt, A, Ebinghaus, R, Brunke, EG, Pfaffhuber, KA, Edwards, G, Howard, D, Powell, J, Keywood, M, Wang, F. 2015. Comparison of mercury concentrations measured at several sites in the Southern Hemisphere. *Atmospheric Chemistry and Physics* **15**: 3125–3133. DOI: https://doi.org/10.5194/acp-15-3125-2015.

Slemr, F, Martin, L, Labuschagne, C, Mkololo, T, Angot, H, Magand, O, Magand, O, Garat, P, Ramonet, M, Bieser, J. 2020. Atmospheric mercury in the Southern Hemisphere - Part 1: Trend and inter-annual variations in atmospheric mercury at Cape Point, South Africa, in 2007–2017, and on Amsterdam Island in 2012–2017. *Atmospheric Chemistry and Physics* **20**: 7683–7692. DOI: https://doi.org/10.5194/acp-20-7683-2020.

Spadaro, JV, Rabl, A. 2008. Global health impacts and costs due to mercury emissions. *Risk Analysis* **28**: 603–613.

Sprovieri, F, Pirrone, N, Bencardino, M, D'Amore, F, Carbone, F, Cinnirella, S, Mannarino, V, Landis, M, Ebinghaus, R, Weigelt, A, Brunke, EG, Labuschagne, C, Martin, L, Munthe, J, Wängberg, I, Artaxo, P, Morais, F, De Melo Jorge Barbosa, H, Brito, J, Cairns, W, Barbante, C, Del Carmen Diéguez, M, Elizabeth Garcia, P, Aurélien, D, Angot, H, Magand, O, Skov, H, Horvat, M, Kotnik, J, Alana Read, K, Mendes Neves, L, Manfred Gawlik, B, Sena, F, Mashyanov, N, Obolkin, V, Wip, D, Bin Feng, X, Zhang, H, Fu, X, Ramachandran, R, Cossa, D, Knoery, J, Maruszczak, N, Nerentorp, M, Norstrom, C. 2016. Atmospheric mercury concentrations observed at ground-based monitoring sites globally distributed in the framework of the GMOS network. *Atmospheric Chemistry and Physics* **16**: 11915–11935. DOI: https://doi.org/10.5194/acp-16-11915-2016.

Steffen, A, Douglas, T, Amyot, M, Ariya, P, Aspmo, K, Berg, T, Bottenheim, J, Brooks, S, Cobbett, F, Dastoor, A, Dommergue, A, Ebinghaus, R, Ferrari, C, Gardfeldt, K, Goodsite, ME, Lean, D, Poulain, A, Scherz, C, Skov, H, Sommar, J, Temme, C. 2008. A synthesis of atmospheric mercury depletion event

chemistry in the atmosphere and snow. *Atmospheric Chemistry and Physics* **8**: 1445–1482. DOI: https://doi.org/10.5194/acp-8-1445-2008.

Tekran: Model 2537A Ambient Mercury Vapour Analyzer User Manual. 2006a. Rev. 3.01, Technical report: Toronto, Canada.

Tekran: Model 2537B Ambient Mercury Vapour Analyzer User Manual. 2006b. Rev. 3.10, Technical report: Toronto, Canada.

Theys, N, Van Roozendael, M, Hendrick, F, Yang, X, De Smedt, I, Richter, A, Begoin, M, Errera, Q, Johnston, PV, Kreher, K, De MaziÃre, M. 2011. Global observations of tropospheric BrO columns using GOME-2 satellite data. *Atmospheric Chemistry and Physics* **11**: 1791–1811. DOI: https://doi.org/10.5194/acp-11-1791-2011.

UNEP. 2018. Global Mercury assessment. Technical Report. UNEP. Available at https://www.unep.org/resources/publication/global-mercury-assessment-2018. Accessed 5 March 2021.

Wang, S, Schmidt, JA, Baidar, S, Coburn, S, Dix, B, Koenig, TK, Apel, E, Bowdalo, D, Campos, TL, Eloranta, E, Evans, MJ, Di Gangi, JP, Zondlo, MA, Gao, RS, Haggerty, JA, Hall, SR, Hornbrook, RS, Jacob, D, Morley, B, Pierce, B, Reeves, M, Romashkin, P, Ter Schure, A, Volkamer, R. 2015. Active and widespread halogen chemistry in the tropical and subtropical free troposphere. *Proceedings of the National Academy of Sciences of the United States of America* **112**: 9281–9286. DOI: https://doi.org/10.1073/pnas.1505142112.